

## Quantum Strong Coupling with Protein Vibrational Modes

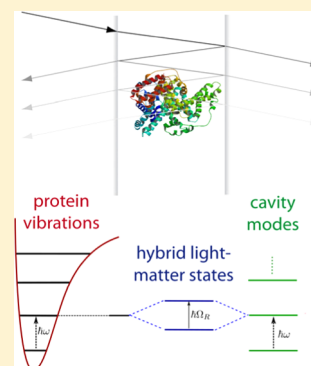
Robrecht M. A. Vergauwe,<sup>†</sup> Jino George,<sup>†</sup> Thibault Chervy,<sup>†</sup> James A. Hutchison,<sup>†</sup> Atef Shalabney,<sup>‡</sup> Vladimir Y. Torbeev,<sup>\*,†</sup> and Thomas W. Ebbesen<sup>\*,†</sup>

<sup>†</sup>University of Strasbourg, CNRS, ISIS, 8 allée Gaspard Monge, 67000 Strasbourg, France

<sup>‡</sup>Department of Physics and Optical Engineering, Ort Braude College, Karmiel 21982, Israel

### Supporting Information

**ABSTRACT:** In quantum electrodynamics, matter can be hybridized to confined optical fields by a process known as light–matter strong coupling. This gives rise to new hybrid light–matter states and energy levels in the coupled material, leading to modified physical and chemical properties. Here, we report for the first time the strong coupling of vibrational modes of proteins with the vacuum field of a Fabry–Perot mid-infrared cavity. For two model systems, poly(L-glutamic acid) and bovine serum albumin, strong coupling is confirmed by the anticrossing in the dispersion curve, the square root dependence on the concentration, and a vacuum Rabi splitting that is larger than the cavity and vibration line widths. These results demonstrate that strong coupling can be applied to the study of proteins with many possible applications including the elucidation of the role of vibrational dynamics in enzyme catalysis and in H/D exchange experiments.



In the past few years, it has become clear that the light–matter strong coupling<sup>1–7</sup> can be employed to alter the physical and chemical properties of molecular systems. Strong coupling of the electronic transition between the ground and first excited state can lead to modulation of photochemical isomerization rates,<sup>8,9</sup> work functions,<sup>10</sup> organic semiconductor conductivity,<sup>11</sup> and a perovskite phase transition.<sup>12</sup> Vibrational strong coupling, VSC, on the other hand, can be employed to modulate the bond vibrations of specific functional groups within a molecule.<sup>13–19</sup> The splitting of a vibrational state into two new (vibro-)polaritonic states leads to a change in the Morse potential and consequently in the (ground state) reactivity of the entire molecule, which holds a great promise for applications in the field of (bio)chemistry. We have recently demonstrated that a basic deprotection reaction of an organic alkynyl silyl compound can be totally modified under VSC in a microfluidic infrared Fabry–Perot cavity.<sup>20</sup>

These effects of strong light–matter interactions are due to the fact that fundamentally this quantum phenomenon involves the hybridization of an electronic or a vibrational transition with the modes of an optical cavity (illustrated in Figure 1A), somewhat akin to the hybridization of s and p atomic orbitals or the formation of molecular orbitals from atomic orbitals during chemical bonding.<sup>21–23</sup> The results are the so-called “dressed” states, which have a mixed light–matter character. Strong coupling arises when a molecular transition is brought in resonance with a photonic cavity mode and when the interaction is faster than any loss mechanism. It is important to note that, as theory predicts, the vacuum field of the optical mode of the cavity (i.e., the zero point energy of the mode) already gives rise to new light–matter states. In other words, the light–matter hybridization occurs even in the dark. When

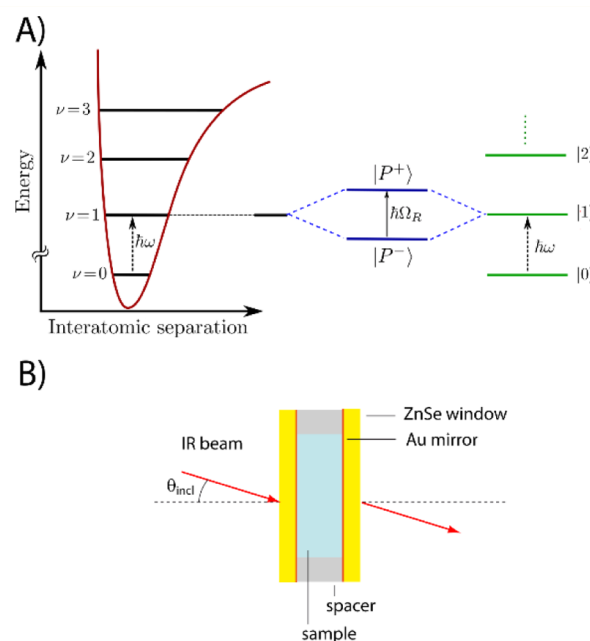


**Figure 1.** Overview of strong coupling and of the experimental approach. (A) Illustration of the principle of vibrational strong coupling. (B) Schematic illustration of the measurement cell.

many molecules are present in a cavity, the resulting dressed states encompass all of the coupled molecules. For a further

Received: August 19, 2016

Accepted: September 30, 2016

Published: September 30, 2016

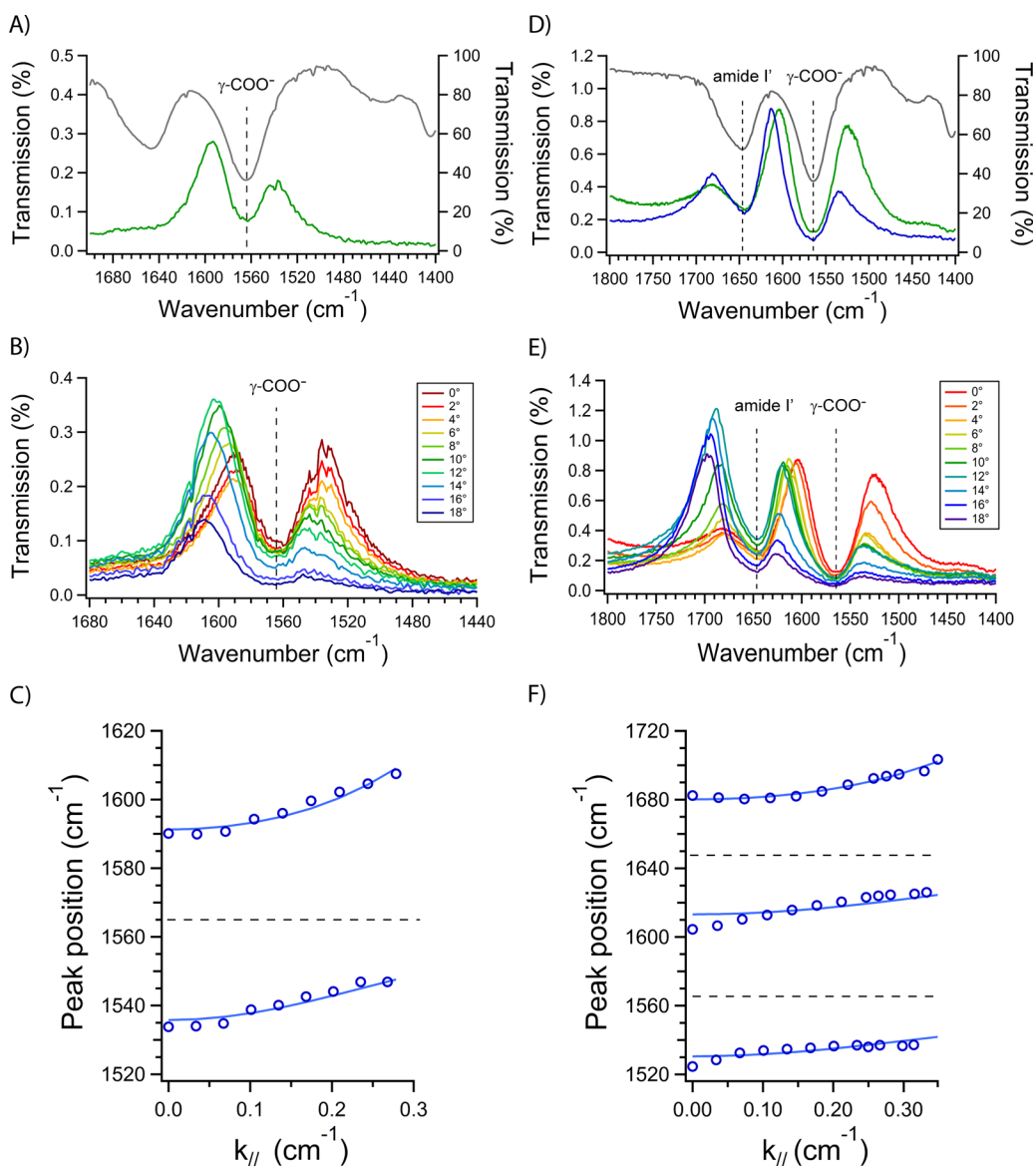


**Figure 2.** FTIR spectra and dispersion data of poly(L-glutamic acid) in a cavity under strong coupling conditions. Deuterated PLGA was inserted into a Fabry–Perot cavity (illustrated in Figure 1B) and measured with FTIR spectrometer. (A–C) Data for PLGA at 5% (w/v). (D–F) Data for PLGA at 15% (w/v). (A,D) IR transmission spectrum for cavity tuned close to either the amide I' or  $\gamma$ -COO<sup>-</sup> asymmetric stretching vibration of PLGA. Green curves: resonance with the  $\gamma$ -COO<sup>-</sup> side-chain asymmetric stretching mode. Blues curve: resonance with the amide I' mode. Gray curves: reference IR transmission spectrum of PLGA outside a cavity. (B,E) Data of the angle-dependent dispersion measurements. IR spectra were recorded for incidence angles between 0° and 18°. (C,F) Dispersion curves with the peak positions of the polariton branches as a function of the magnitude of the in-plane wave vector ( $k_{\parallel}$ ). To avoid misinterpretations, strong coupling dispersion data is preferentially plotted against this component of the wave vector (see Supporting Information for the conversion formula).<sup>22</sup> The measured polariton peak positions are denoted with dark blue open circles and the coupled oscillator model fit with a light blue solid line. The location of the amide I' and  $\gamma$ -COO<sup>-</sup> modes are marked with dashed lines. All measurements were performed in D<sub>2</sub>O.

discussion of the physics of quantum strong light–matter interaction, the reader is referred to one of the reviews<sup>22,23</sup> or to a recent perspective oriented toward molecular and material science.<sup>21</sup>

Although electronic strong coupling of biomolecules has been demonstrated,<sup>24,25</sup> VSC has not yet been achieved to the best of our knowledge.<sup>13,14,20,21</sup> The main challenge in performing VSC of proteins is the 2 orders of magnitude smaller extinction coefficient of vibrational transitions compared to those of electronic transitions, which necessitates the use of very high sample concentrations. To date, the VSC of pure molecular liquids, polymer films, and organic substances

dissolved in solutions has been reported.<sup>13–17,19,26</sup> Working with proteins at very high concentrations can lead to structural and functional alterations and even detrimental effects such as aggregation.<sup>27–30</sup> Here, we demonstrate the vibrational strong coupling of poly(L-glutamic acid) (PLGA) and of bovine serum albumin (BSA) under conditions where the native fold of the latter is largely preserved. The PLGA peptide homopolymer and serum protein are attractive model systems because they are both well characterized, highly water-soluble, and exhibit one or more intense infrared absorption bands (PLGA, amide I and  $\gamma$ -COO<sup>-</sup> asymmetric stretching; BSA, amide I).<sup>27,31,32</sup>

Deuterium-exchanged PLGA dissolved in D<sub>2</sub>O under the conditions used here ( $c = 2.5\text{--}15\%$  (w/v), measured  $pD = 7.6\text{--}7.8$ ) displays an intense amide I' and  $\gamma\text{-COO}^-$  asymmetric stretching bands at  $1647$  and  $1565\text{ cm}^{-1}$ , respectively (Figure 2A and D gray curve). To achieve vibrational strong coupling, Fabry–Perot cavities were fabricated consisting of two parallel ZnSe windows coated with a reflective Au thin film and separated by a spacer (schematically shown in Figure 1B). The transmission spectrum of such an empty cavity exhibits a typical progression of transmission peaks representing the optical modes generated by the cavity (see Supporting Information). After introducing a 5% (w/v) PLGA solution and tuning the cavity resonance close to the PLGA  $\gamma\text{-COO}^-$  mode, the spectral signature of strong light–matter coupling is observed. The transmission spectrum of the sample (shown in Figure 2A, green curve) displays two peaks symmetrically spaced around the peak position of the PLGA  $\gamma\text{-COO}^-$  mode. These two peaks are the spectral signature of the two new polaritonic states (conventionally denoted  $IP+$  and  $IP-$ ). However, in itself this observation does not constitute sufficient proof of strong coupling because a similar splitting can be generated simply by an absorber overlapping with a transmission mode.

For a further confirmation of the presence of strong light–matter coupling, the angle-dependent dispersion of the sample needs to be examined.<sup>13,14,2f,22</sup> Polaritonic states inherit the dispersive properties of the empty cavity with a characteristic anticrossing at the intersection with the absorbing transition resulting in the two polaritonic branches.<sup>21–23</sup> To observe this behavior, the IR spectrum of the sample is measured at different incidence angles of the probe beam in the FTIR. The spectra for PLGA recorded between  $0^\circ$  to  $18^\circ$  are displayed in Figure 2B. The dimensions of the sample holder prohibit investigation of higher angles. As the angle of incidence is varied, the lower branch shifts to higher wavenumbers up to a limiting value and loses intensity. At the same time, the upper branch gains in intensity and disperses to higher wavenumbers.<sup>13,14</sup> When the locations of the peak positions are plotted as a function of the magnitude of the in-plane wave vector ( $k_{\parallel}$ ) of the incoming light (Figure 2C), an anticrossing is indeed observed. Fitting this data with the coupled oscillator model<sup>21–23</sup> allows the extraction of the vacuum Rabi splitting, which is the energy difference between the two new vibro-polariton states at exact resonance. The vacuum Rabi splitting amounts here to  $55.4\text{ cm}^{-1}$ , which corresponds to about 3.5% of the transition energy of the PLGA  $\gamma\text{-COO}^-$  mode. Finally, the strong coupling regime requires that the line width of the bare molecular transition and the cavity mode are both less than the vacuum Rabi splitting.<sup>21–23</sup> This is indeed the case here since they are estimated to be  $45.2$  and  $48.9\text{ cm}^{-1}$ , respectively. Therefore, the strong coupling conditions are all met for this system.

When PLGA at a concentration of 10 or 15% (w/v) is inserted in a cavity near resonance with either the amide I' or  $\gamma\text{-COO}^-$  asymmetric stretching mode of poly(L-glutamic acid), three new bands appear instead of just the two branches expected for the coupling of a single molecular vibration with one cavity mode (see Figure 2D for the data for 15% w/v; see Figure S2D for the data for 10% w/v). Angle-resolved measurements reveal the dispersive behavior of the three branches as shown in Figures 2E–F and S2E–F. The dispersive behavior of the different curves is explained by the simultaneous, independent coupling of both vibrational modes to the cavity vacuum field. This is a common effect when two transitions are close in energy and couple to the same

optical mode.<sup>14,17,33–35</sup> Vacuum Rabi splittings associated with both vibrations are consequently the minimal energy differences between the respective branches.<sup>21–23</sup> Because these Rabi splittings are high compared to the energy difference between the two (bare) transitions, simultaneous coupling occurs even when, for instance, the cavity is blue-detuned with respect to the higher-lying amide I' transition. Comparison of the Rabi splittings with the line widths of the coupled cavity mode and molecular vibrations again confirms that the strong coupling regime is reached. The values are summarized in Table 1. It

**Table 1. Overview of the Cavity Parameters and Measured Vacuum Rabi Splittings**

mode	species	bare vibration line width ( $\text{cm}^{-1}$ )	concentration (% w/v)	cavity mode line width ( $\text{cm}^{-1}$ )	vacuum Rabi splitting ( $\text{cm}^{-1}$ )
$\gamma\text{-COO}^-$	PLGA	48.9	2.5	22.8	41.4
			5	19.3	55.3
			10	32.0	85.6
			15	51.5	96.9
amide I'	PLGA	46.2	10	32.0	81.6
			15	51.5	80.1
	BSA	48.8	10	18.9	67.1

should be noted that the reasons that no secondary splitting is observed at 5% (w/v) PGLA (Figure 2A and B) is due to the fact the coupling was tuned to the  $\gamma\text{-COO}^-$  and that the Rabi splitting is so small that the higher vibro-polariton branch does not reach the amide I' band within the angular range of our experiment. This exemplifies the sensitivity of the observation of strong coupling to cavity detuning.

As the concentration is lowered to 2.5%, a weak branch splitting and a dispersive anticrossing of the  $\gamma\text{-COO}^-$  mode can still be observed for PLGA, but now the polariton splitting energy becomes comparable with the bare absorption band line width (Figure S2A and Table 1). However, this is no longer the case for PLGA at a 1% (w/v) concentration (Figure S2G). Plotting the measured values of the  $\gamma\text{-COO}^-$  mode vacuum Rabi splitting as a function of the square-root of the concentration a straight line is obtained (Figure 3) as expected from theory and previous experimental observations.<sup>13,18,19,21,22</sup> This constitutes a definite proof that strong coupling regime has indeed been reached. Because the amide I' band is less

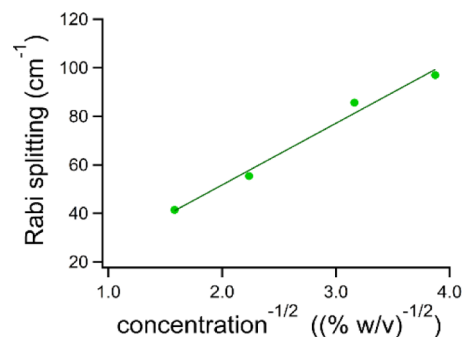


**Figure 3.** Concentration dependence of the vacuum Rabi splitting of the  $\gamma\text{-COO}^-$  stretching mode of poly(L-glutamic acid). The vacuum Rabi splitting for the strongly coupled  $\gamma\text{-COO}^-$  asymmetric stretching modes of PLGA in the four tested conditions are plotted against the square root of the corresponding sample concentration. Linear regression is performed with an  $R^2$  value of 0.985.

intense than the  $\gamma$ -COO<sup>-</sup> stretching band, the threshold for the strong coupling regime will be higher for the former than for the latter.

Although poly(L-glutamic acid) is an adequate polypeptide model sharing many important characteristics with natural proteins (e.g.,  $\alpha$ -helix and  $\beta$ -sheet formation),<sup>31,32</sup> we repeated the coupling of the amide I' vibration with bovine serum albumin which models the properties of a typical globular protein. BSA consists mainly of  $\alpha$ -helical structures and coiled regions, resulting in an amide I' band with a peak observed here at 1646 cm<sup>-1</sup> (in D<sub>2</sub>O at pD = 7.21). After insertion into an IR cavity and tuning the latter into resonance, the typical spectral features of strong light–matter interaction are again observed in the IR transmission spectrum, as can be seen in Figure 4.

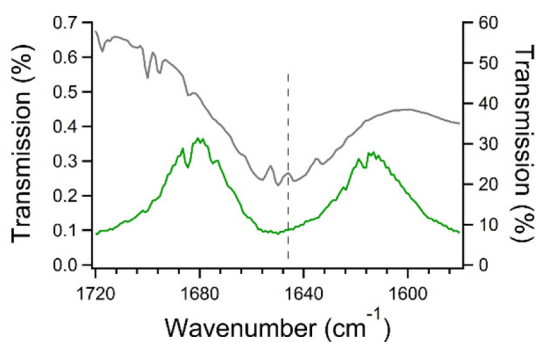


**Figure 4.** FTIR transmission spectrum of bovine serum albumin in a cavity under strong coupling conditions. A 10% (w/v) solution of deuterated BSA in D<sub>2</sub>O was inserted into a Fabry–Perot cavity (illustrated in Figure 1B) tuned to resonance with the amide I' mode of BSA at 1646 cm<sup>-1</sup>.

The vacuum Rabi splitting is estimated at about 67.1 cm<sup>-1</sup>, which amounts to 4.1% of the bare transition energy. The splitting energy is larger than either the bare transition or cavity mode line width (values listed in Table 1), confirming the presence of strong light–matter interaction. However, the concentration employed here is much higher than either those in typical serums (35 to 55 mg/mL) or those used in most applications.<sup>27–29</sup> Studies on protein crowding point out that the effect of BSA on the conformational stability of itself or other proteins is neutral to mildly destabilizing.<sup>28,29</sup> Aggregation and gel formation can also be enhanced in very concentrated BSA solutions.<sup>29</sup> Investigation of BSA in D<sub>2</sub>O at the concentration used for strong coupling and a lower reference concentration (1.6% w/v) using 1D <sup>1</sup>H and 2D <sup>1</sup>H-TOCYSY NMR reveals the preservation of the overall structure (spectra shown in Figure S3). As for aggregation, the shape of the bare amide I' band of BSA does not indicate any significant  $\beta$ -sheets formation or aggregation, neither does the NMR data. Finally, all BSA solutions remained clear during experiments. In summary, strong light–matter interaction regime with BSA can be reached while the protein remains in a near native conformation.

We anticipate that being able to hybridize molecular vibrations of proteins with optical cavity modes is likely to have profound implications for biochemistry and molecular biophysics. Many methods used to study the structure–function relationships of proteins and enzymes often rely on perturbing their chemical composition. A classic example is the use of site-directed mutagenesis or chemical protein synthesis to incorporate single (or multiple) amino acid substitutions

into an existing protein sequence to investigate the effect of substitutions on folding, stability, conformational dynamics or function (e.g., binding or enzymatic activity).<sup>36–41</sup> Our group has recently shown that the ground state reactivity of an organic compound is altered by strong coupling of the molecular vibrations connected to bond being broken.<sup>20</sup> Further studies, both theoretical and experimental, will be necessary to understand the underlying change in the reactivity landscape. Nevertheless, strong coupling of the amide I' bond may also result in a modification of reactivity of amide backbone bonds (e.g., in peptide bond formation, proteolysis reactions, etc.), enzyme catalyzed or otherwise. In addition, strong coupling of amide I' transition can be exploited for H/D exchange to interrogate protein folding dynamics.<sup>42</sup> For enzyme-catalyzed reactions, vibrational strong coupling studies are likely to provide new insights into the vibrational dynamics and energy relaxation involved in such reactions. Previously, molecular bond vibrations in proteins were perturbed by heavy element substitutions and resulted in reduced enzymatic turnover rates.<sup>43,44</sup> VSC could complement such an approach by improving the tunability and selectivity of the perturbation. Going beyond reactivity, the amide protons of the peptide bond take part in noncovalent hydrogen-bonding that stabilizes secondary structures such as  $\alpha$ -helices and  $\beta$ -sheets.<sup>36–41</sup> Amide I band vibration revolve predominantly around stretching of the amide carbonyl,<sup>45</sup> which is an acceptor in such bonding. Similar to deuterium substitution effects on hydrogen-bonding,<sup>46</sup> the hydrogen-bonding interactions with neighboring moieties might also be affected under VSC. Such methodology could then be utilized in studies aiming to modulate the secondary/tertiary/quaternary structure of proteins and enzymes. These examples illustrate how many unexplored possibilities still lie ahead for strongly coupled biomolecular systems which merit further studies.

## ■ EXPERIMENTAL METHODS

Poly(L-glutamic acid) and bovine serum albumin were purchased from Sigma-Aldrich (GmbH, Germany) and deuterated by dissolution in deuterium oxide and lyophilization. All solution pD's were measured by determining the solution pH applying the correction pD = pH + 0.4.<sup>47</sup> NMR spectra of BSA in D<sub>2</sub>O were measured on a 600 MHz Bruker Avance III spectrometer. Fabrication of a Fabry–Perot cavity was done as described in refs 7 and 12. All IR measurements were performed on a Nicolet 6700 FT-IR (Thermo-Fisher Inc., U.S.A.). For each spectrum, 256 interferograms were measured with a 0.964 cm<sup>-1</sup> resolution. Extraction of the polariton peak positions was done by manually fitting of the polariton bands with a Gaussian model. Fitting of the dispersion curves was done with the coupled oscillator model with either 1 or 2 independent excitons in order to retrieve the vacuum Rabi splitting energy. Additional experimental details and information on the data analysis can be found in the Supporting Information.

## ■ ASSOCIATED CONTENT

### Supporting Information

The Supporting Information is available free of charge on the ACS Publications website at DOI: 10.1021/acs.jpcllett.6b01869.

Supplementary methods and materials, empty Fabry–Perot cavity transmission spectrum, spectra and dispersion data 1, 2.5, and 10% (w/w) PLGA, <sup>1</sup>H and <sup>1</sup>H-

TOCSY NMR spectra BSA and examples of curve fitting results for polariton peak extraction. (PDF)

## AUTHOR INFORMATION

### Corresponding Authors

\*E-mail: [ebbesen@unistra.fr](mailto:ebbesen@unistra.fr).

\*E-mail: [torbeev@unistra.fr](mailto:torbeev@unistra.fr).

### Notes

The authors declare no competing financial interest.

## ACKNOWLEDGMENTS

Jérémy Ruiz is gratefully acknowledged for help with preparing the deuterated samples and Anoop Thomas for helpful discussions. We acknowledge support from the International Center for Frontier Research in Chemistry (icFRC, Strasbourg), the ANR Equipex Union (ANR-10-EQPX-52-01), the Labex NIE projects (ANR-11-LABX-0058 NIE) and CSC (ANR-10-LABX-0026 CSC) within the Investissement d'Avenir program ANR-10-IDEX-0002-02.

## REFERENCES

- (1) Abera Guebrou, S.; Symonds, C.; Homeyer, E.; Plenet, J. C.; Gartstein, Y. N.; Agranovich, V. M.; Bellessa, J. Coherent Emission from a Disordered Organic Semiconductor Induced by Strong Coupling with Surface Plasmons. *Phys. Rev. Lett.* **2012**, *108*, 066401.
- (2) Shi, L.; Hakala, T. K.; Rekola, H. T.; Martikainen, J. P.; Moerland, R. J.; Törmä, P. Spatial Coherence Properties of Organic Molecules Coupled to Plasmonic Surface Lattice Resonances in the Weak and Strong Coupling Regimes. *Phys. Rev. Lett.* **2014**, *112*, 153002.
- (3) Berrier, A.; Cools, R.; Arnold, C.; Offermans, P.; Crego-Calama, M.; Brongersma, S. H.; Gómez-Rivas, J. Active Control of the Strong Coupling Regime between Porphyrin Excitons and Surface Plasmon Polaritons. *ACS Nano* **2011**, *5*, 6226–6232.
- (4) Zengin, G.; Johansson, G.; Johansson, P.; Antosiewicz, T. J.; Käll, M.; Shegai, T. Approaching the Strong Coupling Limit in Single Plasmonic Nanorods Interacting with J-Aggregates. *Sci. Rep.* **2013**, *3*, 3074.
- (5) Nagasawa, F.; Takase, M.; Murakoshi, K. Raman Enhancement via Polariton States Produced by Strong Coupling between a Localized Surface Plasmon and Dye Excitons at Metal Nanogaps. *J. Phys. Chem. Lett.* **2014**, *5*, 14–19.
- (6) Hao, Y. W.; Wang, H. Y.; Jiang, Y.; Chen, Q. D.; Ueno, K.; Wang, W. Q.; Misawa, H.; Sun, H. B. Hybrid-State Dynamics of Gold Nanorods/dye J-Aggregates under Strong Coupling. *Angew. Chem., Int. Ed.* **2011**, *50*, 7824–7828.
- (7) Vasa, P.; Wang, W.; Pomraenke, R.; Maiuri, M.; Manzoni, C.; Cerullo, G.; Lienau, C. Optical Stark Effects in J-Aggregate-Metal Hybrid Nanostructures Exhibiting a Strong Exciton-Surface-Plasmon-Polariton Interaction. *Phys. Rev. Lett.* **2015**, *114*, 036802.
- (8) Schwartz, T.; Hutchison, J. A.; Genet, C.; Ebbesen, T. W. Reversible Switching of Ultrastrong Light-Molecule Coupling. *Phys. Rev. Lett.* **2011**, *106*, 196405.
- (9) Hutchison, J. A.; Schwartz, T.; Genet, C.; Devaux, E.; Ebbesen, T. W. Modifying Chemical Landscapes by Coupling to Vacuum Fields. *Angew. Chem., Int. Ed.* **2012**, *51*, 1592–1596.
- (10) Hutchison, J. A.; Liscio, A.; Schwartz, T.; Canaguier-Durand, A.; Genet, C.; Palermo, V.; Samori, P.; Ebbesen, T. W. Tuning the Work-Function via Strong Coupling. *Adv. Mater.* **2013**, *25*, 2481–2485.
- (11) Orgiu, E.; George, J.; Hutchison, J. A.; Devaux, E.; Dayen, J. F.; Doudin, B.; Stellacci, F.; Genet, C.; Schachenmayer, J.; Genes, C.; et al. Conductivity in Organic Semiconductors Hybridized with the Vacuum Field. *Nat. Mater.* **2015**, *14*, 1123–1129.
- (12) Wang, S.; Mika, A.; Hutchison, J. A.; Genet, C.; Jouaiti, A.; Hosseini, M. W.; Ebbesen, T. W. Phase Transition of a Perovskite Strongly Coupled to the Vacuum Field. *Nanoscale* **2014**, *6*, 7243–7248.
- (13) Shalabney, A.; George, J.; Hutchison, J.; Pupillo, G.; Genet, C.; Ebbesen, T. W. Coherent Coupling of Molecular Resonators with a Microcavity Mode. *Nat. Commun.* **2015**, *6*, 5981.
- (14) George, J.; Shalabney, A.; Hutchison, J. A.; Genet, C.; Ebbesen, T. W. Liquid-Phase Vibrational Strong Coupling. *J. Phys. Chem. Lett.* **2015**, *6*, 1027–1031.
- (15) Shalabney, A.; George, J.; Hiura, H.; Hutchison, J. A.; Genet, C.; Hellwig, P.; Ebbesen, T. W. Enhanced Raman Scattering from Vibro-Polariton Hybrid States. *Angew. Chem., Int. Ed.* **2015**, *54*, 7971–7975.
- (16) Long, J. P.; Simpkins, B. S. Coherent Coupling between a Molecular Vibration and Fabry–Perot Optical Cavity to Give Hybridized States in the Strong Coupling Limit. *ACS Photonics* **2015**, *2*, 130–136.
- (17) Muallem, M.; Palatnik, A.; Nessim, G. D.; Tischler, Y. R. Strong Light-Matter Coupling and Hybridization of Molecular Vibrations in a Low-Loss Infrared Microcavity. *J. Phys. Chem. Lett.* **2016**, *7*, 2002–2008.
- (18) Pino, J. D.; Feist, J.; Garcia-Vidal, F. J. Quantum Theory of Collective Strong Coupling of Molecular Vibrations with a Microcavity Mode. *New J. Phys.* **2015**, *17*, 053040.
- (19) Simpkins, B. S.; Fears, K. P.; Dressick, W. J.; Spann, B. T.; Dunkelberger, A. D.; Owrutsky, J. C. Spanning Strong to Weak Normal Mode Coupling between Vibrational and Fabry–Pérot Cavity Modes through Tuning of Vibrational Absorption Strength. *ACS Photonics* **2015**, *2*, 1460–1467.
- (20) Thomas, A.; George, J.; Shalabney, A.; Dryzhakov, M.; Varma, S. J.; Moran, J.; Chervy, T.; Zhong, X.; Devaux, E.; Genet, C.; et al. Ground-State Chemical Reactivity under Vibrational Coupling to the Vacuum Electromagnetic Field. *Angew. Chem., Int. Ed.* **2016**, *55*, 11462–11466.
- (21) Ebbesen, T. W. Hybrid Light–Matter States in a Molecular and Material Science Perspective. *Acc. Chem. Res.* Submitted for publication.
- (22) Törmä, P.; Barnes, W. L. Strong Coupling between Surface Plasmon Polaritons and Emitters: A Review. *Rep. Prog. Phys.* **2015**, *78*, 013901.
- (23) Agranovich, V. M.; Gartstein, Y. N.; Litinskaya, M. Hybrid Resonant Organic–Inorganic Nanostructures for Optoelectronic Applications. *Chem. Rev.* **2011**, *111*, 5179–5214.
- (24) Coles, D. M.; Yang, Y.; Wang, Y.; Grant, R. T.; Taylor, R. A.; Saikin, S. K.; Aspuru-Guzik, A.; Lidzey, D. G.; Tang, J. K.-H.; Smith, J. M. Strong Coupling between Chlorosomes of Photosynthetic Bacteria and a Confined Optical Cavity Mode. *Nat. Commun.* **2014**, *5*, 5561.
- (25) Dietrich, C. P.; Steude, A.; Tropsch, L.; Schubert, M.; Kronenberg, N. M.; Ostermann, K.; Höfling, S.; Gather, M. C. An Exciton-Polariton Laser Based on Biologically Produced Fluorescent Protein. *Sci. Adv.* **2016**, *2*, e1600666.
- (26) Galego, J.; Garcia-Vidal, F. J.; Feist, J. Cavity-Induced Modifications of Molecular Structure in the Strong-Coupling Regime. *Phys. Rev. X* **2015**, *5*, 41022.
- (27) Barbosa, L. R. S.; Ortore, M. G.; Spinuzzi, F.; Mariani, P.; Bernstorff, S.; Itri, R. The Importance of Protein-Protein Interactions on the pH-Induced Conformational Changes of Bovine Serum Albumin: A Small-Angle X-Ray Scattering Study. *Biophys. J.* **2010**, *98*, 147–157.
- (28) Miklos, A. C.; Sarkar, M.; Wang, Y.; Pielak, G. J. Protein Crowding Tunes Protein Stability. *J. Am. Chem. Soc.* **2011**, *133*, 7116–7120.
- (29) Guo, J.; Harn, N.; Robbins, A.; Dougherty, R.; Middaugh, C. R. Stability of Helix-Rich Proteins at High Concentrations. *Biochemistry* **2006**, *45*, 8686–8696.
- (30) Ellis, R. J. Macromolecular Crowding: Obvious but Underappreciated. *Trends Biochem. Sci.* **2001**, *26*, 597–604.
- (31) Itoh, K.; Foxman, B. M.; Fasman, G. D. The Two Beta Forms of Poly(L-Glutamic Acid). *Biopolymers* **1976**, *15*, 419–455.
- (32) Hernik, A.; Puławski, W.; Fedorczyk, B.; Tymecka, D.; Misicka, A.; Filippek, S.; Dzwolak, W. Amyloidogenic Properties of Short  $\alpha$ -L-Glutamic Acid Oligomers. *Langmuir* **2015**, *31*, 10500–10507.

- (33) Lidzey, D. G.; Bradley, D. D. C.; Armitage, A.; Walker, S.; Skolnick, M. S. Photon-Mediated Hybridization of Frenkel Excitons in Organic Semiconductor Microcavities. *Science* **2000**, *288*, 1620–1623.
- (34) Wenus, J.; Parashkov, R.; Ceccarelli, S.; Brehier, A.; Lauret, J. S.; Skolnick, M. S.; Deleporte, E.; Lidzey, D. G. Hybrid Organic-Inorganic Exciton-Polaritons in a Strongly Coupled Microcavity. *Phys. Rev. B: Condens. Matter Mater. Phys.* **2006**, *74*, 235212.
- (35) Hakala, T. K.; Toppari, J. J.; Kuzyk, A.; Pettersson, M.; Tikkanen, H.; Kunttu, H.; Törmä, P. Vacuum Rabi Splitting and Strong-Coupling Dynamics for Surface-Plasmon Polaritons and Rhodamine 6G Molecules. *Phys. Rev. Lett.* **2009**, *103*, 053602.
- (36) Matouschek, A.; Kellis, J. T.; Serrano, L.; Bycroft, M.; Fersht, A. R. Transient Folding Intermediates Characterized by Protein Engineering. *Nature* **1990**, *346*, 440–445.
- (37) O'Neil, K. T.; DeGrado, W. F. How Calmodulin Binds Its Targets: Sequence Independent Recognition of Amphiphilic Alpha-Helices. *Trends Biochem. Sci.* **1990**, *15*, 59–64.
- (38) Clackson, T.; Wells, J. A. A Hot Spot of Binding Energy in a Hormone-Receptor Interface. *Science* **1995**, *267*, 383–386.
- (39) Andrews, F. H.; McLeish, M. J. Using Site-Saturation Mutagenesis to Explore Mechanism and Substrate Specificity in Thiamin Diphosphate-Dependent Enzymes. *FEBS J.* **2013**, *280*, 6395–6411.
- (40) Torbeev, V. Y.; Raghuraman, H.; Hamelberg, D.; Tonelli, M.; Westler, W. M.; Perozo, E.; Kent, S. B. H. Protein Conformational Dynamics in the Mechanism of HIV-1 Protease Catalysis. *Proc. Natl. Acad. Sci. U. S. A.* **2011**, *108*, 20982–20987.
- (41) Torbeev, V. Y.; Hilvert, D. Both the Cis-Trans Equilibrium and Isomerization Dynamics of a Single Proline Amide Modulate  $\beta_2$ -Microglobulin Amyloid Assembly. *Proc. Natl. Acad. Sci. U. S. A.* **2013**, *110*, 20051–20056.
- (42) Englander, S. W.; Mayne, L.; Kan, Z.-Y.; Hu, W. Protein Folding—How and Why: By Hydrogen Exchange, Fragment Separation, and Mass Spectrometry. *Annu. Rev. Biophys.* **2016**, *45*, 135–152.
- (43) Suarez, J.; Schramm, V. L. Isotope-Specific and Amino Acid-Specific Heavy Atom Substitutions Alter Barrier Crossing in Human Purine Nucleoside Phosphorylase. *Proc. Natl. Acad. Sci. U. S. A.* **2015**, *112*, 11247–11251.
- (44) Silva, R. G.; Murkin, A. S.; Schramm, V. L. Femtosecond Dynamics Coupled to Chemical Barrier Crossing in a Born-Oppenheimer Enzyme. *Proc. Natl. Acad. Sci. U. S. A.* **2011**, *108*, 18661–18665.
- (45) Barth, A.; Zscherp, C. What Vibrations Tell about Proteins. *Q. Rev. Biophys.* **2002**, *35*, 369–430.
- (46) Singh, S.; Rao, C. N. R. Deuterium Isotope Effects on Hydrogen Bonding. *Can. J. Chem.* **1966**, *44*, 2611–2615.
- (47) Glasoe, P. K.; Long, F. A. Use of Glass Electrodes To Measure Acidities in Deuterium Oxide. *J. Phys. Chem.* **1960**, *64*, 188–190.